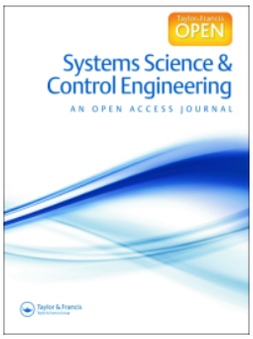

Systems Science & Control Engineering

An Open Access Journal

ISSN: (Print) (Online) Journal homepage: www.tandfonline.com/journals/tssc20

Sensorless control of permanent magnet synchronous motor for exhaust energy recovery of internal combustion engine: a comparison between Kalman filter and MRAS observer

Silvia Di Girolamo, Antonino Sferlazza, Emiliano Pipitone, Salvatore Caltabellotta & Maurizio Cirrincione

To cite this article: Silvia Di Girolamo, Antonino Sferlazza, Emiliano Pipitone, Salvatore Caltabellotta & Maurizio Cirrincione (2024) Sensorless control of permanent magnet synchronous motor for exhaust energy recovery of internal combustion engine: a comparison between Kalman filter and MRAS observer, Systems Science & Control Engineering, 12:1, 2322067, DOI: 10.1080/21642583.2024.2322067

To link to this article: https://doi.org/10.1080/21642583.2024.2322067

Published online: 02 Apr 2024.

SYSTEMS SCIENCE & CONTROL ENGINEERING: AN OPEN ACCESS JOURNAL
2024, VOL. 12, NO. 1, 2322067
https://doi.org/10.1080/21642583.2024.2322067

Taylor & Francis
Taylor & Francis Group

Sensorless control of permanent magnet synchronous motor for exhaust energy recovery of internal combustion engine: a comparison between Kalman filter and MRAS observer

Silvia Di Girolamo[a], Antonino Sferlazza[a], Emiliano Pipitone[a], Salvatore Caltabellotta[a] and Maurizio Cirrincione[b]

[a]Department of Engineering, University of Palermo, Palermo, Italy; [b]School of Information Technology, Engineering, Mathematics, and Physics (STEMP), University of the South Pacific (USP), Laucala Campus, Suva, Fiji

ABSTRACT

This paper deals with the sensorless control of a Permanent Magnet Synchronous Motor (PMSM) to be employed on a turbo-generator to recover the exhaust gas energy of an Internal Combustion Engine (ICE). The main problem with this application is the high rotational speed required by the exhaust gas turbo-generator. Indeed, this implies the difficulty of installing an encoder for speed measurement and control. For this reason, sensorless control is highly recommendable, but, on the other hand, the main sensorless techniques could fail in this peculiar situation because of the high computational effort required compared with the other sensorless applications. Moreover, a good knowledge of the model parameters is necessary. Therefore, the main goal of this paper is to compare two main sensorless techniques for rotational speed measurement, both in the deterministic framework (Model Reference Adaptive System (MRAS) observer) and stochastic framework (Extended Kalman Filter (EKF)), to verify their effectiveness, their computational load, their sensitivity against parameter variation and noisy measurements, and, finally, to present the best solution for the exhaust gas energy recovery from the internal combustion engine.

ARTICLE HISTORY
Received 3 December 2023
Accepted 15 February 2024

KEYWORDS
Exhaust energy recovery; internal combustion engine; Kalman filter; MRAS observer

1. Introduction

Recent concerns about environmental problems and increasingly worrying climate change highlight the need to adopt adequate measures to reduce the consumption of fossil fuels. Nowadays, the recovery of energy and emissions from vehicles equipped with an ICE is a big problem. The European Union must drastically reduce greenhouse gas (GHG) emissions around the world to keep global warming below 2 Celsius-degrees. For this reason, the European Parliament adopted strong measures, with a target of 55% overall GHG emissions reduction (concerning the 1990 level) by 2050 in the European Union. Great attention is paid to the transport sector. The goal is to make vehicles suitable for compliance with current and future environmental regulations by pushing toward market solutions that combine respect for the environment with vehicle fuel savings. As a result, actions are being taken to reduce polluting emissions from road, rail, air, and waterborne transport.

In this context, the authors have conducted a study to investigate and design a system that allows better exploitation of the chemical energy in the fuel used in internal combustion engines. Hybrid electric vehicles (HEV) have proven to be quite competitive, allowing for a significant reduction in fuel consumption compared to traditional Internal combustion engine vehicles (ICEV). As is widely known, the ICE is a consolidated technology that allows the energy contained in the fuel to be converted into mechanical energy. However, internal combustion engines based on Otto or Diesel cycles cannot complete the gas expansion inside the cylinder, thus losing a significant amount of energy, on the order of 20% of the total. As reported in the scientific literature, several solutions have already been studied and proposed to recover the unexpanded gas energy (Aghaali & Ångström, 2015; Alshammari et al., 2019). The most simple approach is represented by common turbocharging, where the unexpanded gas energy is gathered by a gas turbine (usually a radial in-flow turbine) mechanically connected to a compressor to increase the inlet air pressure and engine power. In this system, however, the turbine only provides the mechanical power required by the compressor, which reduces the amount of energy recovered. Moreover, being connected on the same shaft, turbine, and compressor share the same rotational speed, substantially limiting the overall efficiency (in the order of

CONTACT Silvia Di Girolamo silvia.digirolamo01@unipa.it

20-30%). Several other systems can be traced in the scientific literature (Aghaali & Ångström, 2015; Alshammari et al., 2019). In some cases, an electric generator installed on the same turbocharger shaft (Arsie et al., 2015; Hopmann & Algrain, 2003; Millo et al., 2006; Pasini et al., 2016) is employed to recover the amount of energy gathered by the turbine and not used by the compressor: in these cases, the maximum overall efficiency improvements achieved is 6%; another approach is represented by electric turbo-compound systems, where a turbine-generator group is installed downstream the first turbine to recover the exhaust energy not exploited: in this cases (Kant et al., 2015; Mohd Noor et al., 2015) overall efficiency improvements within 4% have been obtained. In Cipollone et al. (2013) and Zhuge et al. (2011), an auxiliary turbo generator is implemented in parallel with the main turbocharger, allowing for efficiency improvements of up to 9%. In the present paper, the authors investigated a different arrangement (Pipitone et al., 2023a), which is particularly suitable for hybrid propulsion architecture.

As shown in Figure 1, the proposed architecture is an innovative compound system in which a suitably designed exhaust gas turbine connected to a proper electric generator converts the unexpanded exhaust gas energy into electric energy delivered to the vehicle storage system. The energy content of the unexpanded gas could significantly improve the overall efficiency of the propulsion system. The difference, compared to other systems, is that in the proposed thermal unit, the entire exhaust gas flow from the combustion engine completes the expansion (from the exhaust pressure of the engine to the pressure of the exhaust pipe) inside the turbine, whose output power is transformed into electricity by the generator. This system is named Separated Electric Compound Engine since, as shown in Figure 1, the compressor used for engine charging is not connected to the turbine employed for exhaust gas energy recovery, thus letting their operating conditions be independent of each other. In the propulsion system proposed, the turbine always operates with the entire engine exhaust mass flow to recover as much energy as possible; on the contrary, the compressor, which is mechanically independent of the turbine, is driven by its electric motor only when supercharging is required, i.e. for the higher engine loads. It is worth noting that, as discussed in previous papers published by the same authors (Pipitone et al., 2023a, 2023b), to comply with the required wide range of mass flow rates and pressure ratio (i.e. the ratio between the turbine inlet and outlet pressure), the exhaust gas turbine adopted is a variable nozzle turbine; this kind of turbine allows an efficient adaptation to several operating conditions (i.e. mass flow rate and pressure ratio) by adequately setting the distributor blade position. The electrical power produced by the turbo-generator group could contribute

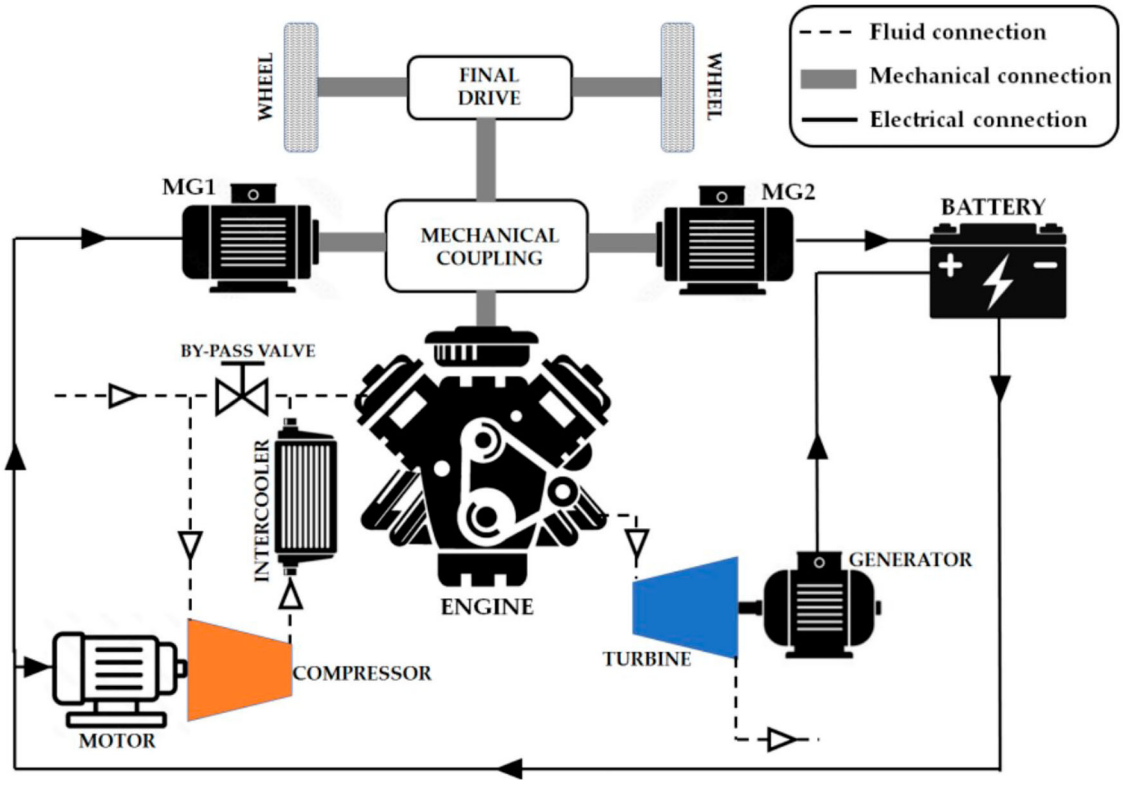

Figure 1. Schematic representation of the separated electric compound system.

to the total power delivered for vehicle traction, thus increasing the vehicle's fuel economy. To increase the performance and reduce the size of the turbo-generator group, high-speed machines are required, as they allow for high-energy density and high efficiency. A permanent magnet synchronous motor (PMSM) is the most common type of electric motor used in hybrid systems. It is also the best choice for high-speed applications as it has a higher energy density and efficiency than conventional induction motors (Gerada et al., 2018).

The main focus of this paper will be the investigation of the feasibility of two main sensorless techniques (EKF and MRAS observer), usually employed for standard PMSM, for the exhaust gas energy recovery from the internal combustion engine. Indeed, there are several aspects to be considered in this application that are not present in classical motor control, i.e. very high speed, high disturbances, parameter variations, etc. Moreover, among the other solutions proposed in the literature, these two types of sensorless control methods were chosen for this work because the EKF is used for stochastic frames, while the MRAS is used for deterministic frames; this allows us to highlight the differences in considering whether the source of randomness explicitly considered in the model gives a benefit.

2. Mathematical model of the high-speed PMSM and related control

This paper will focus on a high-speed permanent magnet synchronous motor (HS-PMSM), analyzing the control system for an efficient exhaust gas energy recovery. As mentioned, in the separated electric compound propulsion system analyzed here, the task of the turbo-generator is to convert the energy of the exhaust gas, which could not complete the expansion in the cylinder, into electrical energy. This energy transformation should be carried out with the maximum possible efficiency. To this purpose, the optimal control of the considered turbo-generator must be performed by acting on two separate parameters, i.e. the distributor nozzle angle and the rotor speed of rotation. In the turbine considered, the nozzle blade position should vary in the narrow range of 2.9−11.2 degrees: the control of this parameter may be performed with a good response time and robustness using a stepper motor. Instead, the rotor speed of rotation is characterized by a wider range of variation (70,000 to 180,000 rpm in the turbine here considered) and, taking into account the rotor inertia. Its control is not as easy as in the case of the nozzle blade angle: it should be performed employing the connected generator, whose rapid and robust control is the focus of the present paper. One of the most common control methods for electrical machine drives is field-oriented control (FOC), also known as vector control, which improves the performance of PMSM drives. In FOC, the speed control of PMSM becomes easy due to the decoupling of the torque component from the flux component. FOC incorporates direct and quadrature axis current controllers and speed proportional-integral (PI) controllers to achieve the required control of the current vector, thus obtaining precise speed and position control. For vector-controlled electrical machine drives, precise motor position measurement is very important. Motor position can be measured using different position sensors, such as encoders or resolvers, and speed sensors to detect the position and speed of the motor, respectively. However, due to limited space, cost, reliability optimization, and their weak robustness in a high-speed region, such sensors can lead to several problems. An alternative practical solution for reducing problems is estimating the rotor position and speed through current and voltage measurements rather than a direct measurement. Hence, sensorless control is widely utilized for electrical machine drive systems, which significantly increases the robustness of the drive itself. In this paper, an EKF estimator and an MRAS observer will be designed. The proposed algorithms will be verified through Matlab/Simulink environment simulations. Before introducing the two sensorless techniques analyzed in this paper, the considered mathematical model of the HS-PMSM is given below. In particular, the set of differential equations describing the behavior of the main variables is:

$$\frac{di_{sd}}{dt} = \frac{1}{L_d}\left(-R_s i_{sd} + \rho\omega L_q i_{sq} + v_d\right), \tag{1a}$$

$$\frac{di_{sq}}{dt} = \frac{1}{L_q}\left(-R_s i_{sq} - \rho\omega L_q i_{sd} - \sigma\omega K_e + v_q\right), \tag{1b}$$

$$\frac{d\omega}{dt} = \frac{1}{J}\left[\frac{3}{2}\left(\rho K_e i_{sq} + \rho(L_d - L_q) i_{sd} i_{sq}\right) - \eta(\omega) - f_v\omega\right], \tag{1c}$$

where i_{sd} and i_{sq}, L_d and L_q, v_d and v_q are the stator currents, inductances, and stator voltage components along the d-q axis, respectively, ρ represents the number of pole pairs, K_e is the flux constant that depends on the magnets, R_s is the stator resistance, J is the moment of inertia, f_v is the viscous friction, and finally, ω indicates the angular velocity of the rotor. Equations (1a) represent the mathematical model of the HS-PMSM in the so-called $d-q$ rotating reference frame (Kulkarni & Thosar, 2013; Morimoto et al., 2001). Note that the saturation, the eddy currents, and the hysteresis losses have been neglected, and the assumption of sinusoidally induced electromagnetic force has been considered. PMSM drives based on FOC have been widely adopted in industrial applications due to their fast and fully decoupled control of torque and

currents (Consoli et al., 2004; Qian et al., 2004; B. Wang et al., 2016). In an FOC-based PMSM drive, the double-loop structure is usually adopted. The internal current loop regulates the stator currents to track their reference, while the external speed loop adjusts the mechanical speed or the generated torque. Thus, the dynamic response and stability of the double-loop are the key factors that determine the dynamic quality of the whole drive system. The details of the FOC are not given since it is not the main focus of this paper. However, the reader is addressed to Vas (1998) for further details.

3. Sensorless control

In HS-PMSM, using sensorless control is a great advantage because it increases the system's overall reliability. The high rotational speed, vibrations, and high temperatures made the encoder susceptible to damage. Therefore, sensorless control represents a necessary solution to overcome these problems, and it allows for reducing the mechanical complexity of the system and operating in hostile environments at high speed by reducing the maintenance requirements. In the literature, several sensorless control techniques exist for PMSM drives (Liang et al., 2017; Morimoto et al., 2001; Qiao et al., 2012; Z. Wang et al., 2012). This paper will analyze two types of sensorless control: the MRAS observer and the EKF estimator. We chose these two types of sensorless control because they are two of the main principal methods in the literature. Moreover, the EKF estimator is used for stochastic frames, while the MRAS observer is used for deterministic frames. In the stochastic frame, the effects of both process and measurement noise are explicitly taken into account, where the state equation and the measured output are corrupted by the stochastic processes. Consequently, the derived estimation algorithm tries to minimize the effects of such a source of randomness. In the deterministic framework, the stochastic effects are not explicitly considered. For this reason, it is interesting to compare them and, in particular, highlight the differences in considering whether the source of randomness explicitly in the model gives a benefit.

3.1. Model reference adaptive system observer

The MRAS observer is one of the most commonly used techniques in sensorless control, as it provides good results, is easy to implement, and gives robustness and an accurate estimate of motor speed (Alonge et al., 2015; Cirrincione et al., 2010; Kim et al., 2003; Kivanc & Ozturk, 2018; Kojabadi & Ghribi, 2006). The MRAS estimator comprises three elements: the reference model,

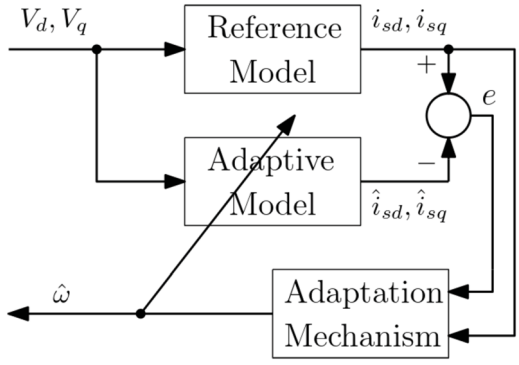

Figure 2. Block diagram of MRAS.

the adaptive model, and the adaptation mechanism, as shown in Figure 2. The reference and the adaptive models are designed to estimate the stator currents along the *d-q* axis but with a significant difference: unlike the adaptive model, the reference model does not require knowledge of the speed to estimate the currents. Therefore, the adaptation mechanism looks for the error between the reference and the adaptive model since the output of the adaptive model is expected to converge with the output of the reference model only if the estimated speed is correct. The physical machine represents the reference model, and the currents are measured. To derive the adaptive model, it is necessary to consider Equations (1a)–(1b). In particular, it can be represented by the following model:

$$\begin{bmatrix} \hat{i}_{sd} \\ \hat{i}_{sq} \end{bmatrix} = \begin{bmatrix} -\frac{R_s}{L_d} & \rho\hat{\omega}\frac{L_q}{L_d} \\ -\rho\hat{\omega}\frac{L_q}{L_d} & -\frac{R_s}{L_q} \end{bmatrix} \begin{bmatrix} \hat{i}_{sd} \\ \hat{i}_{sq} \end{bmatrix} + \begin{bmatrix} \frac{1}{L_d} & 0 \\ 0 & \frac{1}{L_q} \end{bmatrix} \begin{bmatrix} V_d \\ V_q \end{bmatrix} + \begin{bmatrix} 0 \\ -1 \end{bmatrix} \frac{\rho\hat{\omega}K_e}{L_q} \tag{2}$$

where $\hat{i}_{sd}$, $\hat{i}_{sq}$, and $\hat{\omega}$ represent the estimated values of i_{sd}, i_{sq}, and ω, respectively. The adaptive model calculates the same variables as the reference model using the rotor speed value provided by the adaptation mechanism, which is designed to generate the value of the estimated speed used to minimize the stator current errors. To ensure the convergence to zero of the estimation error, the adaptation mechanism is constituted by a PI controller. Moreover, the error considered as input for the PI is represented by the angular difference between the measured and the estimated stator-current space vectors. Therefore, the equation for the estimated speed can be written as follows:

$$\hat{\omega} = \left(K_p + \frac{K_i}{s}\right)\left[\frac{L_q}{L_d} i_{sd}\hat{i}_{sq} - \frac{L_d}{L_q} i_{sq}\hat{i}_{sd} - \frac{K_e}{L_d}(i_{sq} - \hat{i}_{sq})\right], \tag{3}$$

This choice of the adaptation mechanism ensures the stability of the observer, as demonstrated using Popov's theory in Rasvan (2002), where the convergence to zero of the following error dynamics is shown:

$$\dot{e} = Ae - \lambda \tag{4}$$

where $e = [e_{sd}\ e_{sq}]^\top = [(i_{sd} - \hat{i}_{sd})\ (i_{sq} - \hat{i}_{sq})]^\top$,

$$\lambda = J\rho(\omega - \hat{\omega}) \begin{bmatrix} \hat{i}_{sd} & \hat{i}_{sq} \end{bmatrix}^\top, \quad \text{with } J = \begin{bmatrix} 0 & -1 \\ 1 & 0 \end{bmatrix},$$

and finally, A is given by:

$$A = \begin{bmatrix} -\frac{R_s}{L_d} & \rho\omega\frac{L_q}{L_d} \\ -\rho\omega\frac{L_q}{L_d} & -\frac{R_s}{L_q} \end{bmatrix}.$$

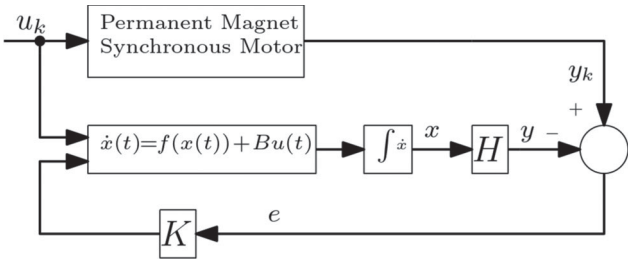

Figure 3. Block diagram of EKF.

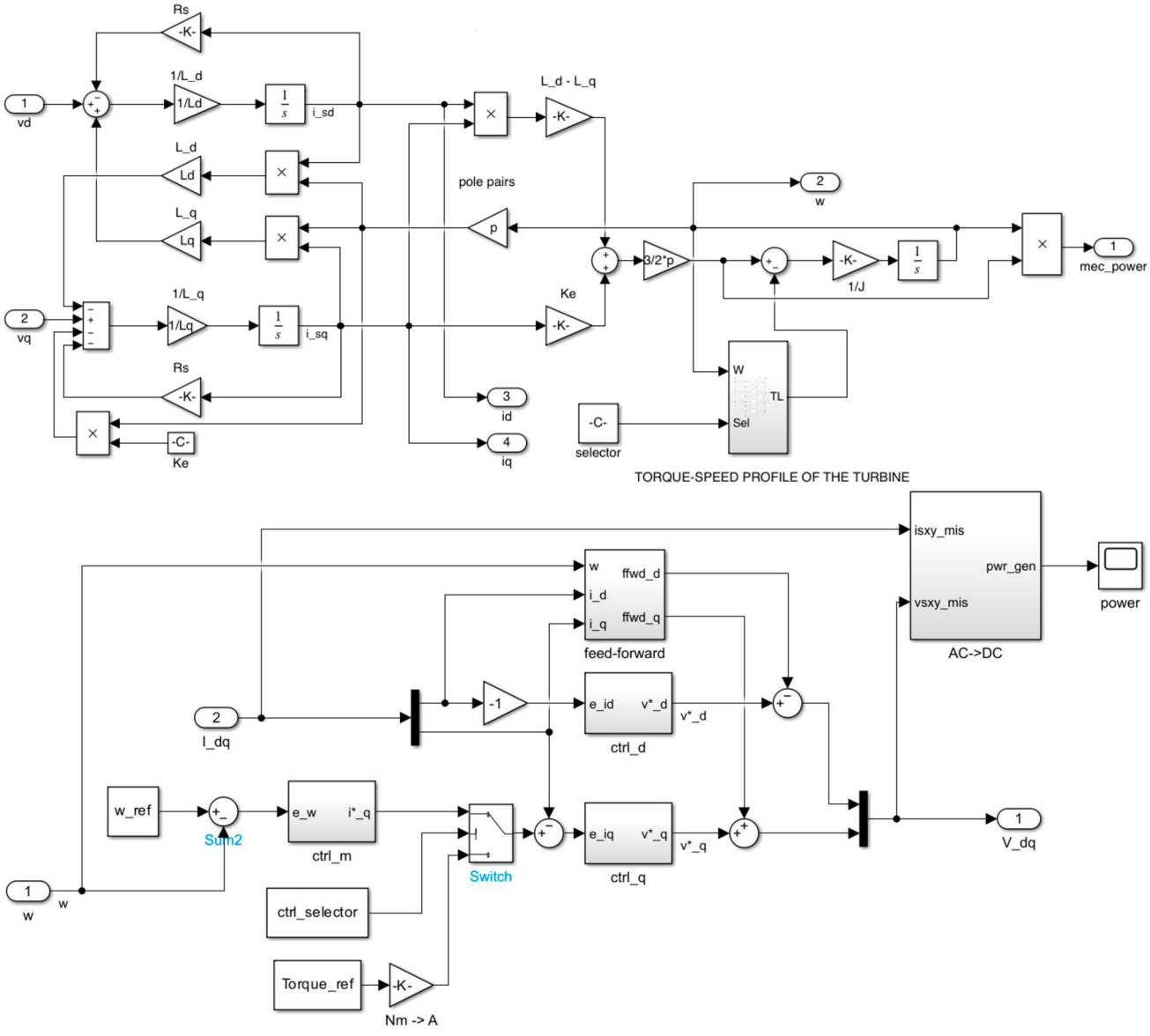

Figure 4. Block diagrams of the electric compound system (upper plot) and of the field-oriented control (bottom plot) in Simulink environment.

Note that the MRAS observer is one of the most common methods due to its simplicity, direct stability approach, and low computational effort; furthermore, it is easy to implement in a Digital Signal Processor (DSP). However, the MRAS method cannot get a satisfying performance in low-speed regions, and it strongly depends on the accuracy of the reference model. These problems are irrelevant to the proposed application since the PMSM is operated at high speed, and the machine constitutes the model reference.

3.2. Extended kalman filter

The Extended Kalman Filter (EKF) is an estimator for nonlinear stochastic systems, where a recursive estimate of the state is obtained through noisy input-output signals and knowledge of the stochastic properties of the measurement and process noises. The scheme of the EKF considered in this work is shown in Figure 3.

Table 1. Motor parameters.

Parameter	Value
Power P	10 kW
Direct (Quadrature) axis inductance $L_d(L_q)$	55 μH
Stator resistance R_s	0.012 Ω
Permanent magnets flux K_e	0.0141 Wb
Pole-pair number ρ	1
Inertia momentum of the rotor-turbine system J	133.2 μKgm^2

The first step in designing an EKF for PMSM is deriving the PMSM stochastic model in the time domain. Starting from Equations (1a) the following model can be obtained:

$$\dot{x}(t) = f(x(t)) + Bu(t) + Qw(t) \tag{5a}$$

$$y(t) = Hx(t) + Rv(t) \tag{5b}$$

where $x(t)$, $u(t)$, and $y(t)$ are the state, the input, and the output vectors, respectively, given by $x = [\,i_{sd},\, i_{sq},\, \omega\,]^\top$, $u = [\,v_d,\, v_q\,]^\top$, $y = [\,i_{sd},\, i_{sq}\,]^\top$, $w(t)$ and $v(t)$ denote system and measurement noise, which are assumed to be Gaussian zero-mean white stochastic processes, and Q and R are diagonals square matrices of suitable dimensions representing the covariance of $w(t)$ and $v(t)$. Note that the choice of Q and R diagonal means that the signals among the components of $w(t)$ and $v(t)$ are uncorrelated. Finally, $f(x(t))$, B, and H are given by:

$$f(x(t)) = \begin{bmatrix} -\dfrac{R_s}{L_d} i_{sd} + \rho\omega \dfrac{L_q}{L_d} i_{sq} \\ -\dfrac{R_s}{L_q} i_{sq} - \rho\omega \dfrac{L_d}{L_q} i_{sq} - \rho\omega \dfrac{K_e}{L_q} \\ \dfrac{3}{2}\dfrac{\rho}{J}(K_e i_{sq} + (L_d - L_q) i_{sq} i_{sd}) - \dfrac{f_v}{J}\omega - \dfrac{\eta(\omega)}{J} \end{bmatrix},$$

$$B = \begin{bmatrix} \dfrac{1}{L_d} & 0 \\ 0 & \dfrac{1}{L_q} \\ 0 & 0 \end{bmatrix}, \quad \text{and} \quad H = \begin{bmatrix} 1 & 0 & 0 \\ 0 & 1 & 0 \end{bmatrix}.$$

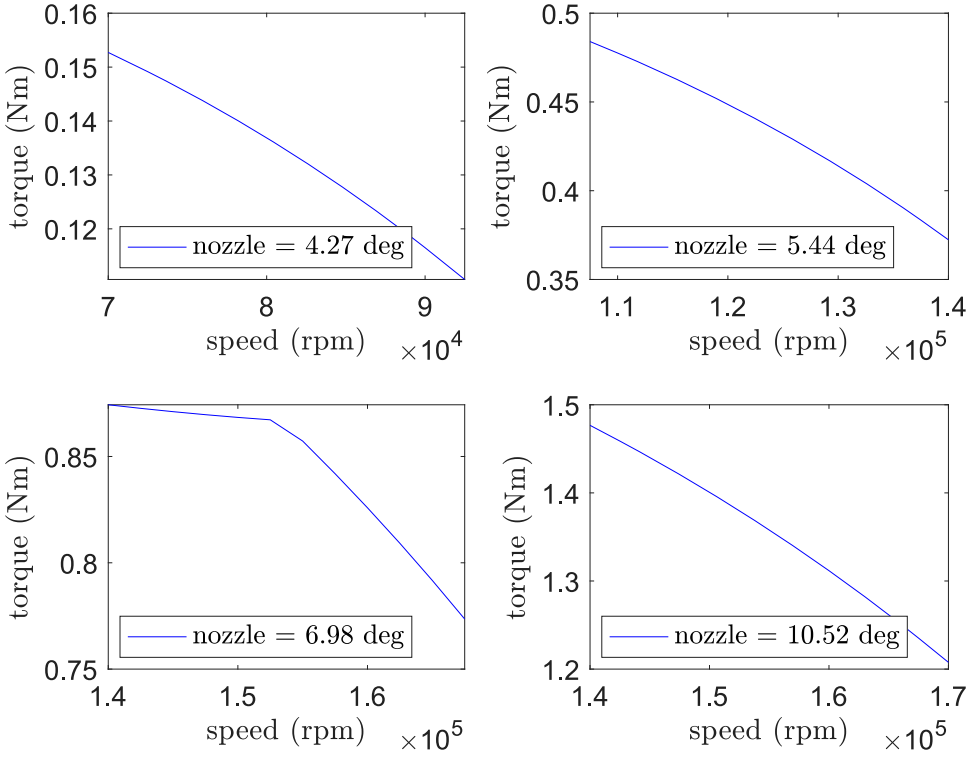

Figure 5. Torque-speed characteristics of the considered turbine.

Note that matrices B and H are constant, while the vector field $f(x(t))$ is time-varying because it depends on the state. To design the EKF, the nonlinear model (5a) can be discretized by applying Euler's method as follows:

$$x_{k+1} = x_k + T_s f(x_k) + T_s B u_k + T_s Q w_k \tag{6a}$$

$$y_k = H x_k + R v_k \tag{6b}$$

where T_s is the sampling time.

The EKF is described by the following recursive algorithm involving the *measurement update* and the *time update* phases. During the kth *measurement update*, the a-posteriori estimates of the state and the covariance matrix of the estimation error P are updated as follows:

$$\hat{x}_{k\,|\,k} = \hat{x}_{k\,|\,k-1} + K_k(y_k - H\hat{x}_{k\,|\,k-1}) \tag{7a}$$

$$P_{k\,|\,k} = P_{k\,|\,k-1} - K_k H P_{k\,|\,k-1} \tag{7b}$$

where $x_{k\,|\,k-1}$ is the predictive estimate of the state at the instant $k-1$, and K_k is the gain of the filter given by:

$$K_k = P_{k\,|\,k-1} H^\top \left(H P_{k\,|\,k-1} H^\top + R \right)^{-1}. \tag{8}$$

Table 2.

Blade angle [°]	Turbine inlet pressure [bar]	Turbine inlet temperature [K]	Rotor speed of rotation [rpm]
4.27	1.705	1006	70000−92500
5.44	2.702	1061	107500−140000
6.98	3.712	1102	140000−167500
10.52	3.938	1115	140000−170000

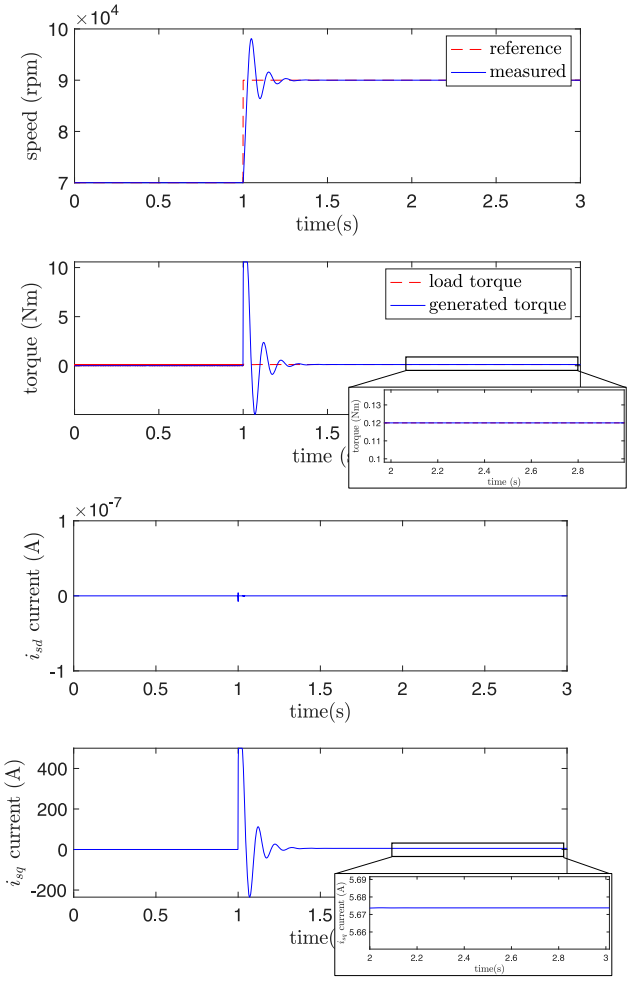

Figure 6. Motor speed ω and torque generated by the motor, and stator current along d-q axis, for the nozzle angle equal to 4.27 during a step variation of the reference speed from 70 to 92.5 krpm.

Table 3. IAE performance indexes.

Blade position angle [°]	Speed tracking error	Estimation error with EKF	Estimation error with MRAS
4.27	105.8	0.6	65.5
5.44	128.8	1.3	179
6.98	116.6	2.3	246.4
10.52	129.9	3.9	282.2

Speed tracking error: $\int_0^T |\omega_{ref}(t) - \omega(t)|dt$ Estimation tracking error: $\int_0^T |\omega(t) - \hat{\omega}(t)|dt$

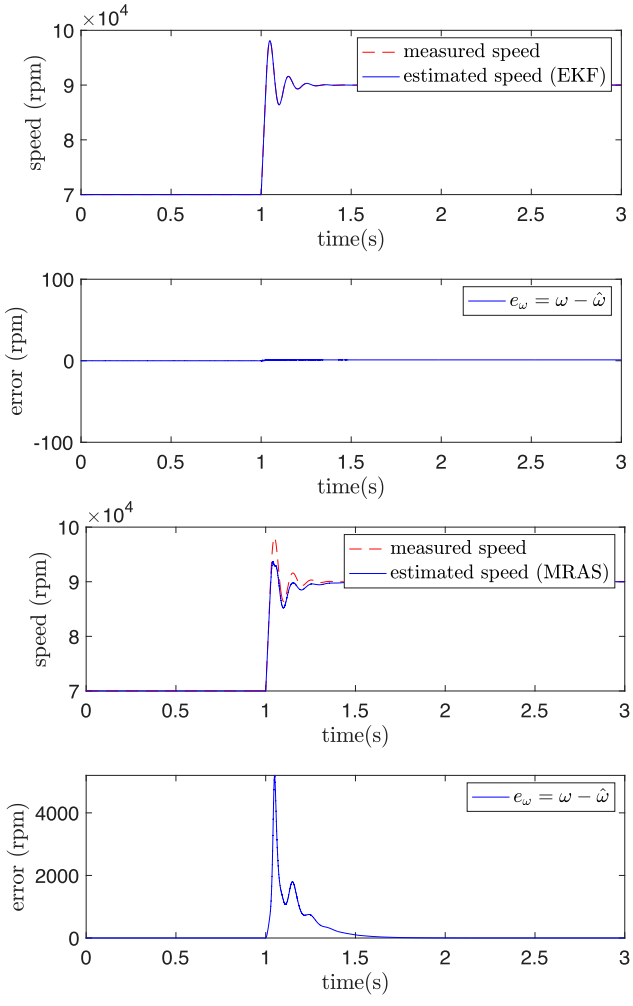

Figure 7. Reference and estimated speed as well as estimation error using EKF, and MRAS, corresponding to the test of Figure 6.

Using $\hat{x}_{k\,|\,k}$ and $P_{k\,|\,k}$, the prediction of the state is computed in the *time update* phase as follows:

$$\hat{x}_{k+1\,|\,k} = f_k(\hat{x}_{k\,|\,k}) + Bu_k \tag{9a}$$

$$P_{k+1\,|\,k} = F_k P_{k\,|\,k} F_k^T + T_s Q \tag{9b}$$

where F_k is the jacobian of the vector field $f(x(t))$ and is given by:

$$F_k = \left.\frac{\partial f_k(x_k)}{\partial x}\right|_{x=\hat{x}_{k\,|\,k}} = \\ = \begin{bmatrix} -\frac{R_s}{L_d} & \rho\omega_{k\,|\,k}\frac{L_q}{L_d} & \rho\frac{L_q}{L_d} i_{sq\,k\,|\,k} \\ -\rho\omega_{k\,|\,k}\frac{L_d}{L_q} & -\frac{R_s}{L_q} & -\rho\left(\frac{K_e}{L_q} + \frac{L_d}{L_q} i_{sd\,k\,|\,k}\right) \\ \frac{3}{2}\frac{\rho}{J}(L_d - L_q) i_{sq\,k\,|\,k} & \frac{3}{2}\frac{\rho}{J}K_e & -\frac{1}{J}\left(f_v - \left.\frac{\partial \eta}{\partial \omega}\right|_{k\,|\,k}\right) \end{bmatrix}.$$

Note that the algorithm automatically selects gain K_k to obtain the best possible estimated state by minimizing the estimation error covariance.

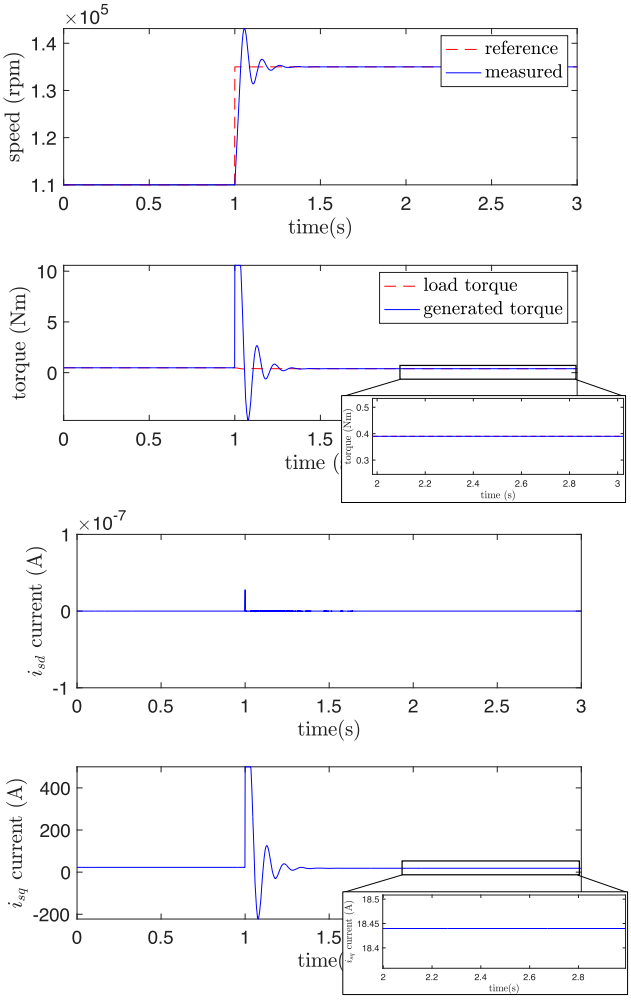

Figure 8. Motor speed ω and torque generated by the motor, and stator current along *d-q* axis, for the nozzle angle equal to 5.44 during a step variation of the reference speed of the motor from 110 to 135 krpm.

Particular attention must be paid to the choice of the machine parameters, the covariance matrices, and initial conditions. The filter is initialized at the instant $k = 0$, with $\hat{x}_{0\,|\,0} = x_0 = [0\ 0\ 0]^\top$ and $P_{0\,|\,0} = P_0 = \alpha I_4$, where α is a constant with a sufficiently high value. Matrices Q and R have been obtained through a suitable preliminary experiment so that the estimated stator currents produced by EKF track the measured ones.

4. Results

The EKF estimator and the MRAS observer have been tested in numerical simulation. In particular, these results aim to verify the effectiveness of the proposed estimators, highlight strengths and weaknesses, their sensitivity against noise and parameter variations, and finally, their computational load. All these characteristics will allow us to define the best estimator to apply for exhaust gas energy recovery in ICE.

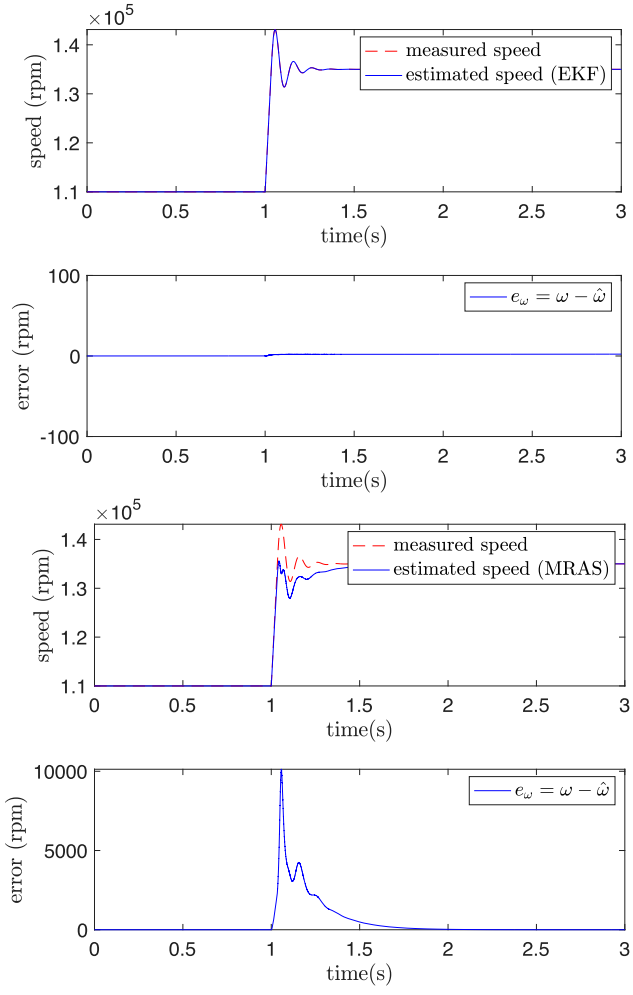

Figure 9. Reference and estimated speed as well as estimation error using EKF, and MRAS, corresponding to the test of Figure 8.

The entire drive system has been implemented in a Matlab-Simulink environment. The Simulink model includes the HS-PMSM model (1a), which embeds the turbine system, the vector FOC control, the EKF estimator, and the MRAS observer. The block diagrams of the electric compound system and of the field-oriented control in the Simulink environment are shown in Figure 4, while the block diagrams of the speed estimators are compliant with those ones shown in Figures 3 and 4. The nominal parameters of the implemented PMSM are given in Table 1. The PI controllers of the FOC are tuned with the following parameters: the proportional and integral constants of the inner loop PI controllers are selected equal to 100 and 6000 respectively, while the parameters of the speed PI controller are equal to 0.2 (proportional constant) and 25 (integral constant). The sampling frequency of estimators is initially set to 5 MHz, but it has been reduced gradually to check the minimum sampling frequency for each estimator. The results of this test will be better described in Subsection 4.2 about the computational load.

To implement the MRAS observer, the following values of K_p and K_i are chosen for the PI-based adaptation mechanism: $K_p = 20$ and $K_i = 200$. Both the EKF estimator and the MRAS observer were simulated in the same environment and conditions, and both inputs of the MRAS observer and EKF are affected by zero-mean white noise.

Regarding the implementation of the EKF, as said in the previous section, the parametrization of the covariance matrices of the observation noise R and of the process noise Q, as well as of the initial covariance matrix P_0 of the estimation error, is a non-trivial task. In the literature, the values of the matrices Q and R are often computed based on a trial-and-error procedure (Rasvan, 2002), in order to minimize the estimation error. This procedure

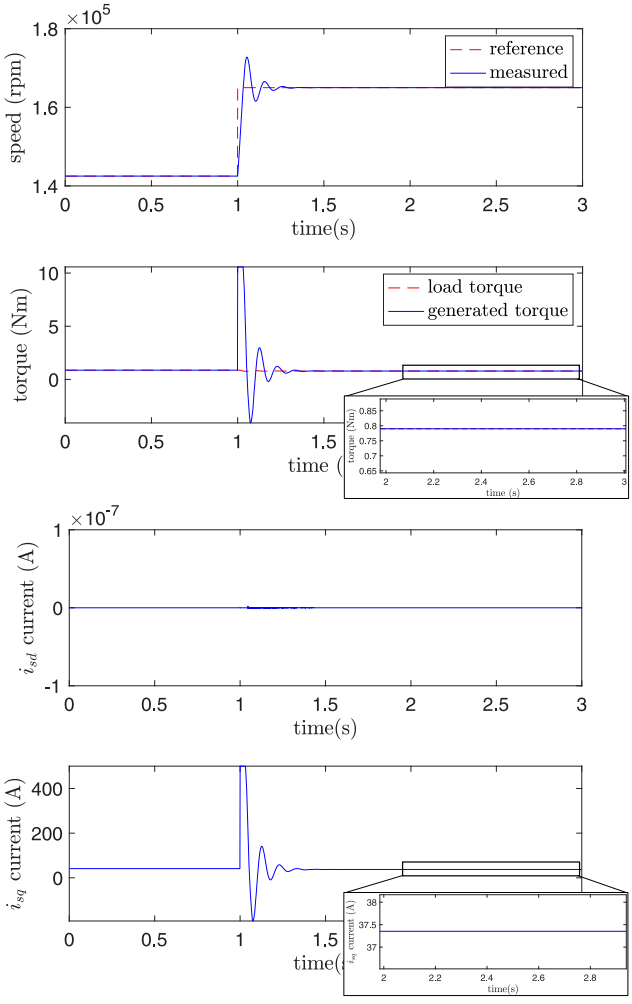

Figure 10. Motor speed ω and torque generated by the motor, and stator current along d-q axis, for the nozzle angle equal to 6.98 during a step variation of the reference speed of the motor from 143 to 168 krpm.

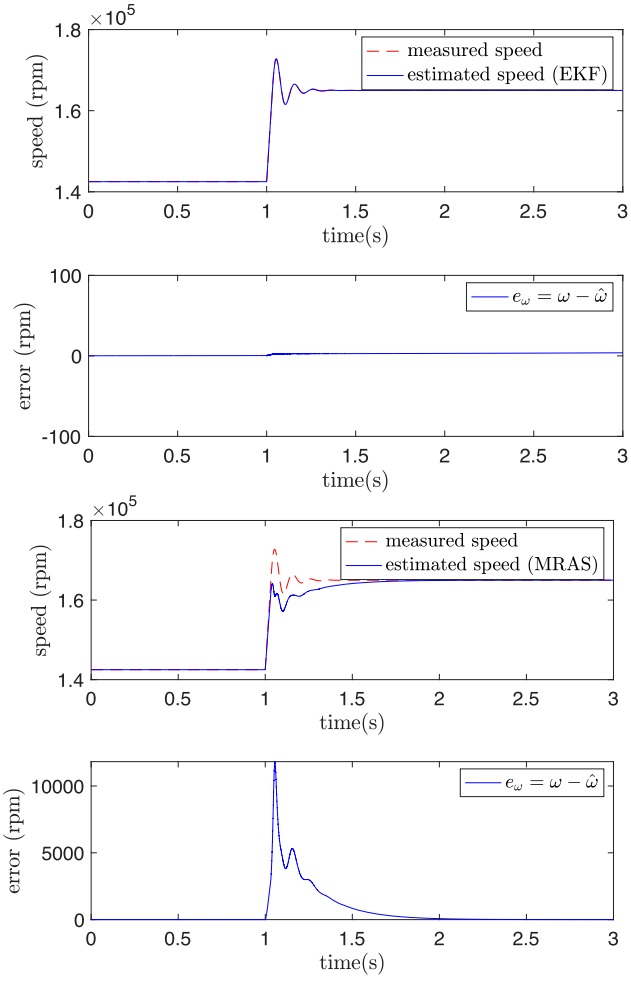

Figure 11. Reference and estimated speed as well as estimation error using EKF, and MRAS, corresponding to the test of Figure 10.

was used also in this case. $P_0 = \text{diag}\{2, 2, 0.05, 1\}$ was chosen, a variance of $R = \text{diag}\{4, 4\}$ was adopted for the measurement noise, and finally, for the parametrization of the covariance matrix representing the process noise, it was found that $Q = \text{diag}\{40^3, 40^3, 40^4\}$ worked fine for this application.

The proposed system has been tested in four turbine operating conditions corresponding to four different nozzle positions. Figure 5 shows the turbine's torque-speed characteristics for the nozzle angles: 4.27, 5.44, 6.98, and 10.52 degrees. Note that these waveforms represent the function $\eta(\omega)$ in Equation (1c), and they were obtained considering, for each nozzle blade position, constant pressure and temperature at the turbine inlet. In contrast, the turbine outlet pressure was supposed to be 1.05 bar independently of the operating conditions (see Table 2). The control has been tested for each blade position, supposed to perform the maximum allowed rotational speed variation (4th column in Table 2). Figure 6 shows the results for the nozzle angle equal to 4.27 during a step variation of the reference speed of the motor from 70 to 92.5 krpm. In particular, the motor speed and the stator currents, i_{sd}, i_{sq}, are shown. Figure 7 shows the estimated speed as long as the estimation error using EKF (upper plot) and MRAS (bottom plot). From these two figures, it is evident that both sensorless systems work, and they can be used in the proposed application. However, the EKF behaves better during transient since it presents an almost zero error. This is due to the adaptation mechanism of the MRAS, which reduces the bandwidth of the observer. At the same time, in the EKF, the gain is automatically selected close to the optimal value to minimize the covariance of the estimation error. Table 3 shows the integral absolute error (IAE) indexes for this test, confirming the above-given comments. Figures 8 and 9 show identical waveforms but using a nozzle angle of 5.44 and

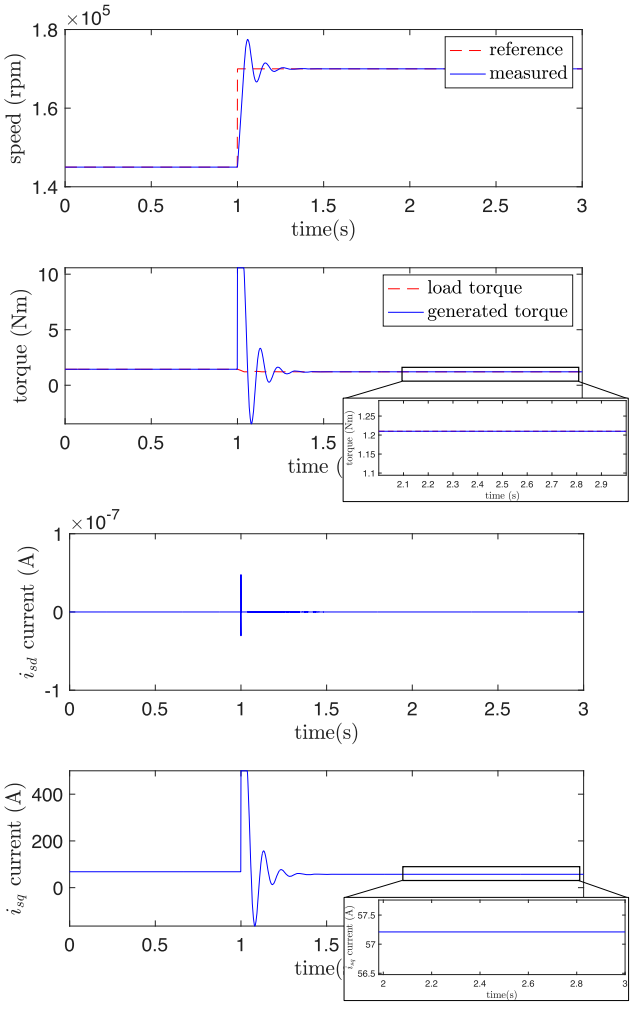

Figure 12. Motor speed ω and torque generated by the motor, and stator current along *d-q* axis, for the nozzle angle equal to 10.52 during a step variation of the reference speed of the motor from 145 to 170 krpm.

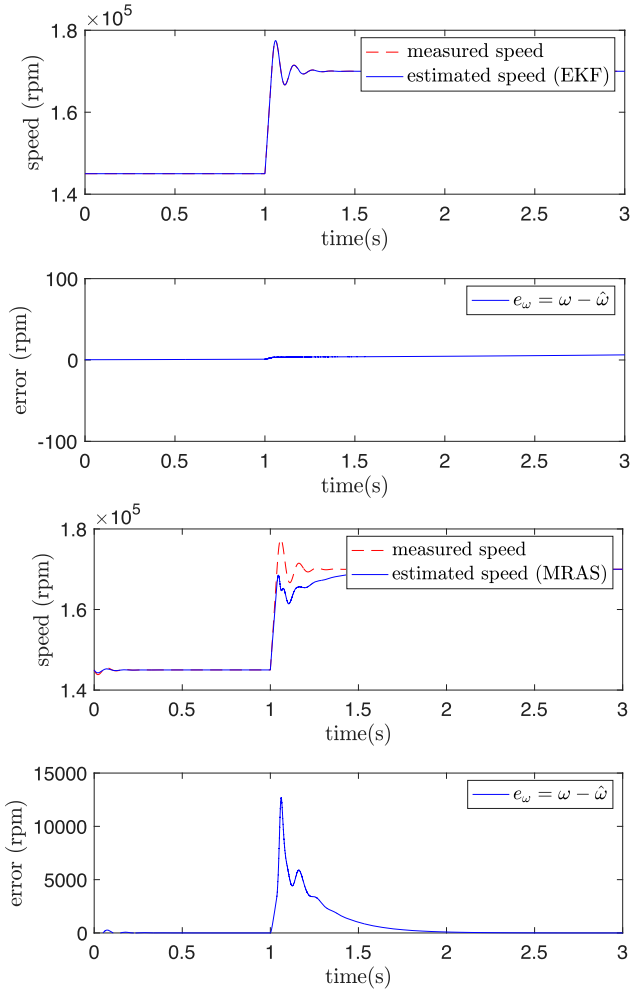

Figure 13. Reference and estimated speed as well as estimation error using EKF, and MRAS, corresponding to the test of Figure 12.

a step variation of the reference speed of the motor from 107.5 to 140 krpm is considered. In Figures 10 and 11, the nozzle angle is set equal to 6.98, and a step variation of the reference speed of the motor from 140 to 167.5 krpm is considered. Finally, the last test is shown in Figures 12 and 13 where the nozzle angle is set equal to 10.52 and the step variation of the reference speed of the motor is from 140 to 170 krpm.

All these figures show that both EKF and MRAS systems work, but it is evident that the error increments when higher nozzle angles are considered, which is valid for both EFK and MRAS. However, by looking at Table 3, we note that this error increment is, in percentage, almost the same for the two estimators, but the absolute value is much higher in MRAS than EKF. This means that very high speeds are critical in the MRAS, while, in the EKF, it does not represent a problem.

4.1. Robustness and sensitivity analysis

To evaluate the sensitivity analysis of the proposed estimators against parameter variations, a simulation has been carried out by detuning the parameters of EKF and MRAS. In particular, the stator resistance R_s and the moment of inertia J are varied within $\pm$ 20%. Indeed, the stator resistance could vary with the temperature, and the inertia could vary with the gas density. In this case, the third turbine operating condition, corresponding to a nozzle angle equal to 6.98, has been considered. The results are shown in Figures 14 and 15, and, in particular, Figure 14 refers to a 20% decrement of R_s and J, while Figure 15 refers to a 20% increment of the same parameters. By evaluating the results, it is evident that both estimators work even when the model parameters are varied, and this confirms that both estimation methods are robust against disturbances.

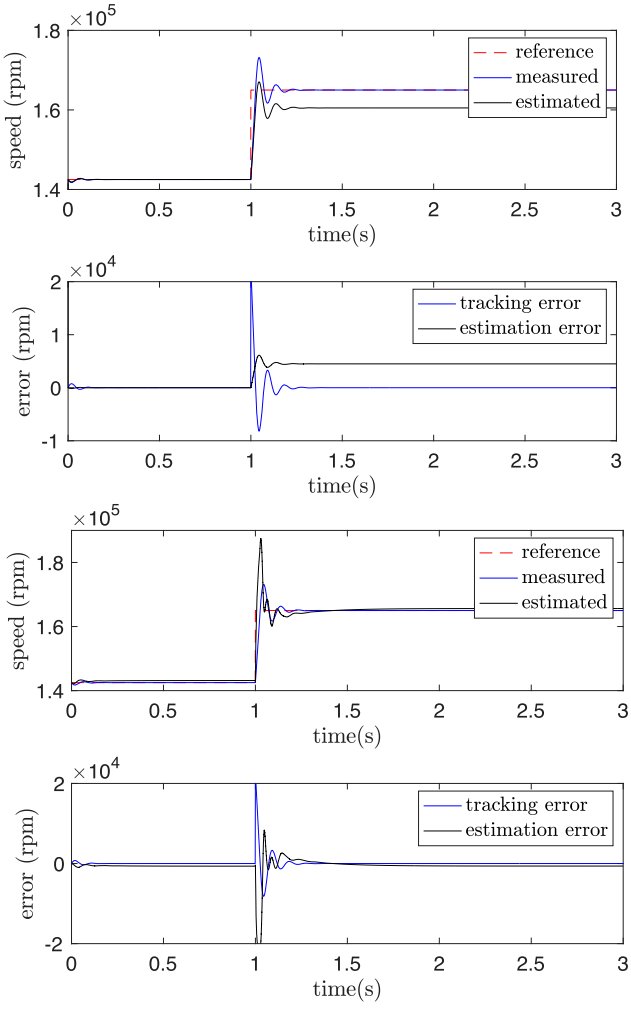

Figure 14. EKF and MRAS responses when R_s and J are decreased by 20%, for the third operating condition.

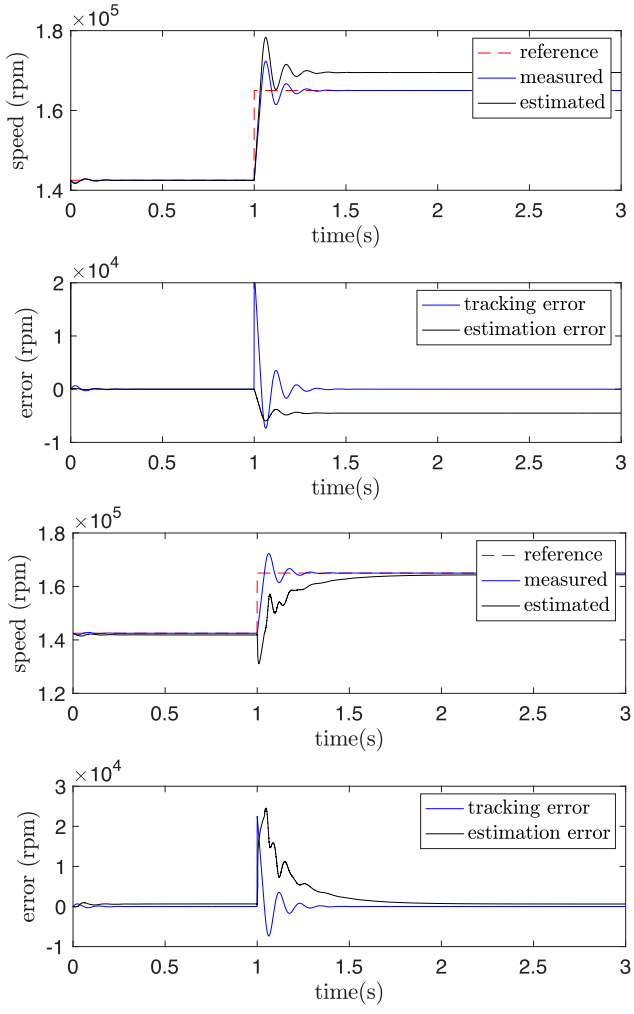

Figure 15. EKF and MRAS responses when R_s and J are increased by 20%, for the third operating condition.

However, comparing EKF with MRAS, we note that EKF performs better during the transient time since the bandwidth of the MRAS is reduced by the adaptation mechanism, but, on the other side, EKF presents a steady-state error that cannot be neglected if accurate speed control is required. Indeed MRAS's steady-state error is almost zero, while the EKF's steady-state error is almost 3%. This highlights that MRAS is more robust against parameter variations than EKF.

4.2. Computational load

Regarding the computational load, the sampling frequency of the estimators initially set to 5 MHz has been reduced to check the minimum value that allows the correct operation of both estimators. From the results, we found that the MRAS sampling frequency has to be greater than (or equal to) 5 MHz; otherwise, during the step variation, the estimator dynamics are insufficient to track the actual speed. Conversely, the minimum frequency achievable with the EKF is 20 kHz, which is much lower than the MRAS case. However, the computational load for each step is much more significant in the EKF than in MRAS since the MRAS's structure is simple and requires few calculations. In contrast, the EKF requires heavy calculations that embed matrix products and inverses. This means that even if the minimum sampling frequency achievable with EKF is lower than MRAS, they are almost equivalent from the computational load point of view.

5. Conclusion

This paper proposes a sensorless control system based on an EKF and an MRAS for an HS-PMSM connected to a radial turbine to recover the exhaust gas energy from an internal combustion engine. Both EKF and MRAS have been designed to estimate the state of the PMSM during different operating conditions, whose estimation property was evaluated through simulations in the Matlab-Simulink environment. The two observers are studied and compared in the same operating conditions to extract their advantages and drawbacks. Simulation results show that both sensorless systems work and can be used in the proposed application. However, the EKF behaves better during transient since it presents an almost zero error concerning MRAS. Regarding the robustness against parameters and load variations, both observers can work under detuned working conditions. However, EKF performs better during the transient time, but, on the other side, EKF presents a steady-state error that must be addressed if accurate speed control is required, and in this last case, the MRAS solution seems the better. Finally, they are almost equivalent from the computational point of view because the minimum sampling frequency achievable with EKF is lower than MRAS. Still, the computational load for each step is much more significant in the EKF than in MRAS.

Disclosure statement

No potential conflict of interest was reported by the author(s).

Funding

This work was supported by Department of Engineering—University of Palermo: FFR_D26_PREMIO_GRUPPO_RICERCA_2020_PIPITONE.

References

Aghaali, H., & Ångström, H.-E. (2015). A review of turbocompounding as a waste heat recovery system for internal combustion engines. *Renewable and Sustainable Energy Reviews*, *49*, 813–824. https://doi.org/10.1016/j.rser.2015.04.144

Alonge, F., Cirrincione, M., Pucci, M., & Sferlazza, A. (2015). Input–output feedback linearization control with on-line mras-based inductor resistance estimation of linear induction motors including the dynamic end effects. *IEEE Transactions on Industry Applications*, *52*(1), 254–266. https://doi.org/10.1109/TIA.2015.2465939

Alshammari, M., Alshammari, F., & Pesyridis, A. (2019). Electric boosting and energy recovery systems for engine downsizing. *Energies*, *12*(24), 4636. https://doi.org/10.3390/en12244636

Arsie, I., Cricchio, A., Pianese, C., Ricciardi, V., & De Cesare, M. (2015). Evaluation of co2 reduction in si engines with electric turbo-compound by dynamic powertrain modelling. *IFAC-PapersOnLine*, *48*(15), 93–100. https://doi.org/10.1016/j.ifacol.2015.10.014

Cipollone, R., Di Battista, D., & Gualtieri, A. (2013). Turbo compound systems to recover energy in ice. *International Journal of Engineering and Innovative Technology*, *3*(6), 249–257.

Cirrincione, M., Pucci, M., Sferlazza, A., & Vitale, G. (2010). Neural based MRAS sensorless techniques for high performance linear induction motor drives. In *IECON – Annual Conference on IEEE Industrial Electronics Society* (pp. 918–926). IEEE.

Consoli, A., Scarcella, G., & Testa, A. (2004). Slip-frequency detection for indirect field-oriented control drives. *IEEE Transactions on Industry Applications*, *40*(1), 194–201. https://doi.org/10.1109/TIA.2003.821804

Gerada, D., Huang, X., Zhang, C., Zhang, H., Zhang, X., & Gerada, C. (2018). Electrical machines for automotive electrically assisted turbocharging. *IEEE Transactions on Mechatronics*, *23*(5), 2054–2065. https://doi.org/10.1109/TMECH.2018.2849081

Hopmann, U., & Algrain, M. C. (2003). *Diesel engine electric turbo compound technology*. SAE Technical Paper, Tech. Rep.

Kant, M., Romagnoli, A., Mamat, A. M., & Martinez-Botas, R. F. (2015). Heavy-duty engine electric turbocompounding. *Proceedings of the Institution of Mechanical Engineers, Part D: Journal of Automobile Engineering*, *229*(4), 457–472.

Kim, Y. S., Kim, S. K., & Kwon, Y. A. (2003). MRAS based sensorless control of permanent magnet synchronous motor. In *SICE – Annual Conference* (Vol. 2, pp. 1632–1637). IEEE.

Kivanc, O. C., & Ozturk, S. B. (2018). Sensorless pmsm drive based on stator feedforward voltage estimation improved with mras multiparameter estimation. *IEEE Transactions on Mechatronics*, *23*(3), 1326–1337. https://doi.org/10.1109/TMECH.3516

Kojabadi, H. M., & Ghribi, M. (2006). MRAS-based adaptive speed estimator in PMSM drives. In *IEEE International Workshop on Advanced Motion Control* (pp. 569–572). IEEE.

Kulkarni, S., & Thosar, A. (2013). Mathematical modeling and simulation of permanent magnet synchronous machine. *International Journal of Electronics and Electrical Engineering*, *1*(2), 66–71. https://doi.org/10.12720/ijeee

Liang, D., Li, J., Qu, R., & Kong, W. (2017). Adaptive second-order sliding-mode observer for pmsm sensorless control considering vsi nonlinearity. *IEEE Transactions on Power Electronics*, *33*(10), 8994–9004. https://doi.org/10.1109/TPEL.2017.2783920

Millo, F., Mallamo, F., Pautasso, E., & Mego, G. G. (2006). *The potential of electric exhaust gas turbocharging for hd diesel engines*. SAE Technical paper, Tech. Rep.

Mohd Noor, A., Che Puteh, R., Rajoo, S., Basheer, U. M., M. H. Md Sah, & Shaikh Salleh, S. H. (2015). Simulation study on electric turbo-compound (etc) for thermal energy recovery in turbocharged internal combustion engine. *Applied Mechanics and Materials*, *799–800*, 895–901. https://doi.org/10.4028/www.scientific.net/AMM.799-800

Morimoto, S., Kawamoto, K., Sanada, M., & Takeda, Y. (2001). Sensorless control strategy for Salient-pole PMSM based on extended EMF in rotating reference frame. In *IEEE Industry Applications Conference* (vol. 4, pp. 2637–2644). IEEE.

Pasini, G., Lutzemberger, G., Frigo, S., Marelli, S., Ceraolo, M., Gentili, R., & Capobianco, M. (2016). Evaluation of an electric turbo compound system for si engines: A numerical approach. *Applied Energy*, *162*, 527–540. https://doi.org/10.1016/j.apenergy.2015.10.143

Pipitone, E., Caltabellotta, S., Sferlazza, A., & Cirrincione, M. (2023a). Hybrid propulsion efficiency increment through exhaust energy recovery – part 1: Radial turbine modelling and design. *Energies*, *16*(3), 1030. https://doi.org/10.3390/en16031030

Pipitone, E., Caltabellotta, S., Sferlazza, A., & Cirrincione, M. (2023b). Hybrid propulsion efficiency increment through exhaust energy recovery – part 2: Numerical simulation results. *Energies*, *16*(5), 2232. https://doi.org/10.3390/en16052232

Qian, W., Panda, S. K., & Xu, J.-X. (2004). Torque ripple minimization in pm synchronous motors using iterative learning control. *IEEE Transactions on Power Electronics*, *19*(2), 272–279. https://doi.org/10.1109/TPEL.2003.820537

Qiao, Z., Shi, T., Wang, Y., Yan, Y., Xia, C., & He, X. (2012). New sliding-mode observer for position sensorless control of permanent-magnet synchronous motor. *IEEE Transactions on Industrial Electronics*, *60*(2), 710–719. https://doi.org/10.1109/TIE.2012.2206359

Rasvan, V. (2002). Popov theories and qualitative behavior of dynamic and control systems. *European Journal of Control*, *8*(3), 190–199. https://doi.org/10.3166/ejc.8.190-199

Vas, P. (1998). *Sensorless vector and direct torque control*. Oxford university press.

Wang, B., Chen, X., Yu, Y., Wang, G., & Xu, D. (2016). Robust predictive current control with online disturbance estimation for induction machine drives. *IEEE Transactions on Power Electronics*, *32*(6), 4663–4674. https://doi.org/10.1109/TPEL.2016.2602853

Wang, Z., Lu, K., & Blaabjerg, F. (2012). A simple startup strategy based on current regulation for back-emf-based sensorless control of pmsm. *IEEE Transactions on Power Electronics*, *27*(8), 3817–3825. https://doi.org/10.1109/TPEL.2012.2186464

Zhuge, W., Huang, L., Wei, W., Zhang, Y., & He, Y. (2011). *Optimization of an electric turbo compounding system for gasoline engine exhaust energy recovery*. Tech. Rep.